Soft Matter

PAPER

View Article Online
View Journal | View Issue

Cite this: *Soft Matter*, 2024, **20**, 4007

Lipidation alters the phase-separation of resilin-like polypeptides†

Zhe Zhang,[a] Jingjing Ji,[b] Md. Shahadat Hossain,[c] Briah Bailey,[d] Shikha Nangia *[b] and Davoud Mozhdehi *[ae]

Biology exploits biomacromolecular phase separation to form condensates, known as membraneless organelles. Despite significant advancements in deciphering sequence determinants for phase separation, modulating these features *in vivo* remains challenging. A promising approach inspired by biology is to use post-translational modifications (PTMs)—to modulate the amino acid physicochemistry instead of altering protein sequences—to control the formation and characteristics of condensates. However, despite the identification of more than 300 types of PTMs, the detailed understanding of how they influence the formation and material properties of protein condensates remains incomplete. In this study, we investigated how modification with myristoyl lipid alters the formation and characteristics of the resilin-like polypeptide (RLP) condensates, a prototypical disordered protein with upper critical solution temperature (UCST) phase behaviour. Using turbidimetry, dynamic light scattering, confocal and electron microscopy, we demonstrated that lipidation—in synergy with the sequence of the lipidation site—significantly influences RLPs' thermodynamic propensity for phase separation and their condensate properties. Molecular simulations suggested these effects result from an expanded hydrophobic region created by the interaction between the lipid and lipidation site rather than changes in peptide rigidity. These findings emphasize the role of "sequence context" in modifying the properties of PTMs, suggesting that variations in lipidation sequences could be strategically used to fine-tune the effect of these motifs. Our study advances understanding of lipidation's impact on UCST phase behaviour, relevant to proteins critical in biological processes and diseases, and opens avenues for designing lipidated resilins for biomedical applications like heat-mediated drug elution.

Received 27th March 2024,
Accepted 16th April 2024

DOI: 10.1039/d4sm00358f

rsc.li/soft-matter-journal

Introduction

Cells use liquid–liquid phase separation (LLPS) of biomacromolecules to form membraneless organelles, a process similar to the phase separation of incompatible macromolecules into condensates.[1,2] These condensates are increasingly used for diverse applications, ranging from the enrichment and encapsulation of biologics[3,4] to underwater adhesives,[5] among others.[6–9] More recently, inspired by the regulatory function of naturally occurring membraneless organelles in cells, such condensates have been explored for cellular and metabolic engineering applications.[10–12] Protein-based condensates are promising candidates for these applications because their sequence and concentration within cells can be tightly regulated; and integrating functional domains into these condensates through genetic fusion is straightforward. However, to advance the design of protein-based condensates for these *in vivo* applications, we still need a deeper understanding of the molecular properties driving phase separation and the ability to dynamically regulate these properties in response to cellular conditions.

While our understanding of the molecular and sequence determinants of phase separation is growing rapidly, the adaptive modulation of these molecular features, especially in complex *in vivo* environments, remains challenging. This difficulty arises because most features—such as conformational disorder,[13] charge patterning,[14] protein sequence,[15] and molecular weight[16]—are genetically predetermined and difficult to alter after protein expression. Although techniques like proteolytic digestion[17] or the use of programmable oligomerization domains[18,19] provide some level of control, there is a need for a

[a] *Department of Chemistry, Syracuse University, Syracuse, New York 13244, USA. E-mail: dmozhdeh@syr.edu*
[b] *Department of Biomedical and Chemical Engineering, Syracuse University, Syracuse, New York 13244, USA. E-mail: snangia@syr.edu*
[c] *Department of Pharmaceutical Technology, University of Dhaka, Bangladesh*
[d] *Department of Biomedical Engineering, Augusta University, Augusta, Georgia 30912, USA*
[e] *BioInspired Syracuse: Institute for Material and Living Systems, Syracuse University, Syracuse, NY 13244, USA*

† Electronic supplementary information (ESI) available: Materials and methods section, supplementary tables, supplementary figures. See DOI: https://doi.org/10.1039/d4sm00358f

more versatile toolkit to adaptively alter the formation and properties of condensates in response to changes in cellular conditions.

Here, nature offers an ingenious solution. Instead of changing the sequence of proteins, cells use post-translational modifications (PTMs) to alter the physicochemistry of modified amino acids.[20] These modifications regulate the location, structure, function, and life cycle of proteins. Therefore, it is not surprising that PTMs are emerging as one of the primary regulators of biological condensates—as they enable the selective (de)activation of interactions that control the formation, properties, and structural complexity of membraneless organelles.[21,22] Due to the well-recognized role of electrostatic interactions in modulating protein phase-separation, the significance of 'charge-altering' PTMs is under intense investigation and is beginning to come into a sharper focus. These include but are not limited to, serine phosphorylation,[23,24] arginine-methylation,[25] and lysine acetylation,[26] which modify multivalent electrostatic interactions by altering coulombic charges or their distributions. However, more than 300 types of PTMs have been identified, and many do not alter the electrostatic charge significantly. The effect of these uncharged PTMs, such as lipidation, on the formation and material properties of protein condensates remains an open question. Unravelling these structure–property relationships can unlock the substantial unrealized potentials of PTMs—as a design space orthogonal to amino acids sequence—for adaptive regulation of phase separation in both *in vivo* and *in vitro* settings.

Among uncharged PTMs, lipidation is a particularly promising modification for several reasons. First, it is one of the most ubiquitous PTMs in eukaryotic cells, and it is well-established that the physicochemistry of the lipid and the architecture of the lipidation site can influence complex biological processes such as cell signalling and apoptosis.[27] Second, the distinct hydrophobicity of lipids can induce supramolecular multivalency in phase-separating polymers *via* short-range attractive interactions that are complementary to better-studied long-range electrostatic interactions.[28] Such alterations could significantly influence the properties of condensates. Third, recent advances in genetic engineering have facilitated the biosynthesis of sequence-defined lipidated proteins, opening new opportunities to establish structure–property relationships for these hybrid biopolymers, explore how lipidation affects protein phase separation, and develop innovative biomaterials.[29]

Our current understanding of lipidation's effects on protein phase separation primarily stems from studies on lipidated elastin-like polypeptides (ELPs).[30,31] ELPs are artificial intrinsically disordered proteins (IDPs) that exhibit lower-critical solubility temperature (LCST) behaviour.[32] However, this LCST behaviour is not typical of most biological phase-separating proteins, which often display the converse property, upper critical solubility behaviour (UCST) *in vitro*.[13] This discrepancy suggests that principles derived from ELP studies may not fully apply to other proteins, indicating a significant knowledge gap regarding the effect of lipidation on UCST phase transition. This paper aims to address this gap by investigating how lipidation and the sequence of lipidation sites impact the formation and material characteristics of resilin-like polypeptides (RLPs) as a model protein with UCST phase transition (Fig. 1).

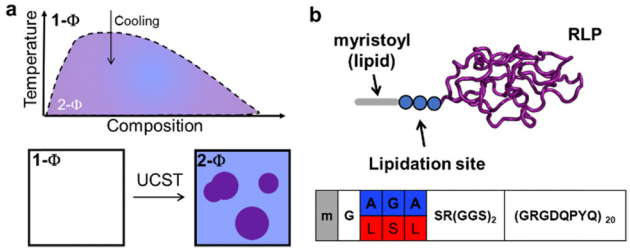

Fig. 1 Schematic phase diagram and architecture of proteins in this study. (a) A homogeneous solution of RLP in buffer (1 − Φ) undergoes spontaneous phase separation upon cooling below its phase boundaries, forming a suspension of two immiscible phases (2 − Φ): protein-rich condensates in a protein-poor solvent. (b) Disordered RLP sequence in purple, with two distinct lipidation sites, differing by three amino acids (in blue and red). Each lipidation site can be modified with a myristoyl group (grey).

In this study, we focused on a model RLP variant based on 20 repeats of octapeptide (GRGDQPYQ), which is compositionally similar to resilin, a natural elastomeric protein found in insect cuticles.[33–35] Resilin contains high levels of aromatic, charged, and polar amino acids and exhibits UCST phase transition. For the model lipid, we chose the myristoyl group, a C14 : 0 fatty acid, appended to the N-terminal glycine of proteins by the *N*-myristoyltransferase (NMT) enzyme. Like many other PTM-installing enzymes, NMT has a broad substrate scope and can modify a large subset of proteins bearing the G-A2-A3-A4-S/T motif.[36] Here, 'G' is the modified residue, the A2/A4 positions have a slight preference for hydrophobic residues, A3 can be occupied by a variety of residues, and the fifth position has a strong preference for serine or threonine.

Guided by these preferences, we selected two NMT substrates with three amino acid differences to analyse if variations downstream of the modification site can also influence how lipidation alters the phase separation of RLPs. Both substrates contain the NMT recognition motifs but incorporate different combinations of hydrophobic and polar amino acids at specific positions. The first motif, 'GAGAS', comprises alanine at positions A2 and A4, with glycine at A3. The second motif, 'GLSLS', includes larger hydrophobic leucine residues at A2 and A4, and a hydrogen-bonding serine at A3. Our aim was to assess if changes to the physicochemical properties of the downstream residues influence the impact of lipidation—specifically investigating the interplay between the sequence of the lipidation site and the effect of lipidation on the UCST phase behaviour of RLPs.

In this study, we first establish that the model RLP, fused to various lipidation sites, can be biosynthetically lipidated in *E. coli*. Employing a range of biophysical and microscopy techniques, we show that lipidation enhances the phase separation propensity of RLPs. Moreover, it significantly alters the dynamics and fluidity of RLP condensates, with the degree of these changes highly dependent on the lipidation site sequence. Molecular simulations and hydropathy analysis suggest that these effects result from modified hydration levels

stemming from the interplay between the physicochemistry lipid and the lipidation site. Finally, we discuss the implications of these findings, emphasizing their relevance to the design and understanding of biomolecular condensates and phase separation processes.

Results

All four constructs, two unmodified RLPs (referred to as *AGA*-RLP and *LSL*-RLP) and their lipidated isoform (referred to as m-*AGA*-RLP and m-*LSL*-RLP), were produced recombinantly in *E. coli* BL21(DE3) strain. For the lipidated constructs, we co-expressed the corresponding RLPs with *S. cerevisiae* NMT (uniport P14743), while supplementing the expression medium with myristic acid. To purify these constructs, we utilized a two-step strategy. First, their temperature-triggered phase-behaviour was used to isolate RLPs (unmodified and/or lipidated) from the endogenous proteins. This initial phase-based purification was followed by reverse-phase high-performance liquid chromatography (RP-HPLC) to separate unmodified and lipidated isoforms to homogeneity. The purified products were characterized using SDS-PAGE, analytical HPLC, mass-spectrometry and NMR to verify their purity and identity (Fig. S1–S5, ESI†).

We first used variable-temperature turbidimetry to characterize the UCST phase-behaviour of unmodified and lipidated RLPs. Lipidation increased the cloud-point of RLPs, and the magnitude of this increase was dependent on the sequence of the lipidation site. A representative turbidimetry plot for *AGA*-RLP and m-*AGA*-RLP (20 μM in PBS) is shown in Fig. 2a. For both proteins, the turbidity of the solution starts to increase rapidly as the temperature is decreased below a critical threshold. The UCST cloud points (marked with an arrow in Fig. 2a), marking the transition from a single miscible phase to a biphasic system, exhibit an increase from 20 °C to 42 °C upon lipidation, suggesting that lipidation increases the propensity of resilin to phase separate. Intriguingly, although both *LSL*-RLP and *AGA*-RLP had similar T_c, the lipidation increased the cloud point of m-*LSL*-RLP to 58 °C (Fig. S6, ESI†). Control experiments showed that these differences are not due to the variation in the concentration of proteins (Fig. S7, ESI†), but are attributable to variations in lipidation sites as discussed more extensively below. Moreover, the lipidation did not affect the reversibility of the phase-separation of RLPs (Fig. S8, ESI†).

To gain insight into the mechanism of phase separation, we investigated the variation of the cloud point with protein concentration, since concentration dependencies can reveal whether phase separation is driven by intra- or intermolecular events. Fig. 2b shows the dilute branch of the phase diagram, where a linear increase in the cloud point is observed with the natural log of the protein concentration (consistent with the empirical observations for ELPs[37] and RLPs[11,12,33]). Specifically, unmodified *AGA*-RLP and *LSL*-RLP showed slopes of 7.7 °C (95% confidence interval (CI): [7.3, 8.1]) and 8.1 °C (CI: [7.7, 8.4]), respectively, while lipidated versions, m-*AGA*-RLP and m-*LSL*-RLP, displayed slopes of 11.7 °C (CI: [10.5, 13.2]) and

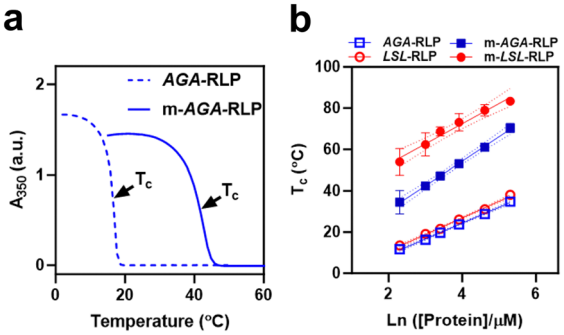

Fig. 2 Characterization of UCST phase behaviour and concentration-dependence of cloud temperatures for unmodified and lipidated RLPs. (a) Representative variable-temperature turbidimetry plots for *AGA*-RLP (dashed line) and m-*AGA*-RLP (solid line) at 20 μM in PBS. Both constructs exhibited UCST behaviour, with a sharp increase in solution turbidity once the temperature was reduced below their respective cloud temperature (T_c). (b) Partial temperature-composition phase diagrams, illustrating the dilute branch of the phase diagram. Lipidation enhanced the phase separation propensity of RLPs, but the extent of this effect depended on the sequence of the lipidation sites. Error bars are standard deviations from two independent measurements, while the dashed line represents the 95% confidence interval of the linear regression.

9.8 °C (CI: [7.4, 12.1]). Importantly, we observed that lipidated RLPs maintained their concentration-dependence in their cloud point temperatures—a finding contrasting with the effects of lipidation on ELPs, where it notably decreases the slope of temperature-composition diagrams.[38,39] Additionally, a notable difference was observed in the *Y*-intercepts of these lines, which underscores the synergistic interaction between the sequence of the lipidation site and the lipid. Here, the *Y*-intercept values for *AGA*-RLP and *LSL*-RLP were determined to be −6.4 °C (CI: [−7.9, −4.9]) and −5.3 °C (CI: [6.8, −3.8]), respectively. Lipidation dramatically shifted these intercepts to 11.9 °C (CI: [1.7, 12.2]) for m-*AGA*-RLP and to 33.4 °C (CI: [24.3, 42.5]) for m-*LSL*-RLP, highlighting the significant impact of the lipidation site on phase behaviour. Together, this data indicates that simply fusing a short peptide sequence to a construct does not significantly alter the propensity of RLP to phase-separate from solution; yet, upon lipidation, the sequence's influence becomes significant. Moreover, this indicates that the lipid moiety's interactions with the surrounding environment are complex, and the context (sequence) of the lipidation site may impact temperature-dependent behaviours, potentially through structured assemblies or by modifying the hydration levels of residues within the sequence.

To elucidate the thermodynamic underpinnings of observed variations in cloud points, we employed a modified Van 't Hoff model on our turbidity data to extract thermodynamic parameters, ΔH and ΔS of phase separation (See ESI† and Fig. S9 for details of analysis).[40] The non-lipidated constructs exhibited similar enthalpic (-93 ± 2 kcal mol^{-1}) and entropic (-230 ± 7 cal mol^{-1} K^{-1}) contributions, indicating that the presence of a short lipidation sequence alone does not significantly alter phase separation thermodynamics and that RLP phase separation is energetically favoured by protein–protein interactions but entropically disfavoured due to the reduced entropy of

polymer chains upon demixing. In contrast, lipidation introduced substantial variations in these thermodynamic parameters, with changes distinctly dependent on the lipidation site sequence. For instance, m-*AGA*-RLP exhibited a decrease in both the enthalpic and entropic components of phase separation, while m-*LSL*-RLP showed a significant increase, suggesting that the synergy between the lipid and the lipidation site can profoundly influence phase separation energetics. Specifically, the enthalpy for m-*AGA*-RLP was reduced by approximately 25% to -73 ± 3 kcal mol^{-1}, with m-*LSL*-RLP showing a much higher phase separation enthalpy (-120 kcal mol^{-1}), and the entropies for m-*AGA*-RLP and m-*LSL*-RLP diverged to -140 and -249.6 cal mol^{-1} K^{-1}, respectively. These findings imply that lipidation, particularly with the LSL sequence, not only affects the enthalpic favourability of phase separation but also seems to modulate the entropic components, potentially by reorganizing the polypeptide chain both in the single-phase region ($T >$ UCST) and within condensates ($T <$ UCST).

To investigate the impact of lipidation (and lipidation site) on RLP assemblies, DLS was utilized to track the hydrodynamic radius (Rh) as a function of temperature while cooling the samples from above to below UCST (Fig. 3a), see Fig. S11 (ESI†) for a representative autocorrelation function for each constructs at a temperature above and below UCST. Consistent with the turbidimetry data, a notable increase in Rh was observed for all constructs as temperature was decreased below their UCST. Importantly, lipidation increased Rh at $T >$ UCST (relative to unmodified RLPs), with the sequence at the lipidation site dictating the extent of this increase. For instance, in the absence of lipidation, constructs transitioned sharply from 4 nm (unimers) to 2500 nm near the UCST, indicative of condensate formation. In contrast, lipidated constructs exhibited significantly larger sizes than unimers at $T >$ UCST, with *m-LSL*-RLP ~180 nm and m-*AGA*-RLP and m-*LSL*-RLP forming assemblies around 45 nm and 180 nm, respectively, pointing to enhanced intermolecular interactions. As temperatures dropped below their respective UCSTs, Rh increased in lipidated constructs. However, the transition to meso-scale assemblies below the UCST was less abrupt, resulting in differently sized assemblies—around 800 nm for m-*AGA*-RLP and 2000 nm for m-*LSL*-RLP. Cognizant of the DLS's constraints in determining the precise sizes of assemblies larger than 1 μm, the trend in the DLS data supports our hypothesis that lipidation and the lipidation site sequence can modulate the thermodynamics of UCST phase separation by affecting protein assembly, thereby impacting the entropic component of phase separation.

DLS results pointed to the formation of large micron-size aggregates at $T <$ UCST, falling within the size range amenable to light microscopic techniques. Consequently, to visualize and further examine these assemblies, we fluorescently labelled RLPs with AZDye™ 488 cadaverine (see ESI† for details) and utilized confocal fluorescent microscopy. This analysis demonstrated that non-lipidated RLPs form canonical condensate droplets, unaffected in overall morphology by the small peptide sequence at the lipidation site (Fig. S10, ESI†). However, a striking difference was observed in the condensates of two

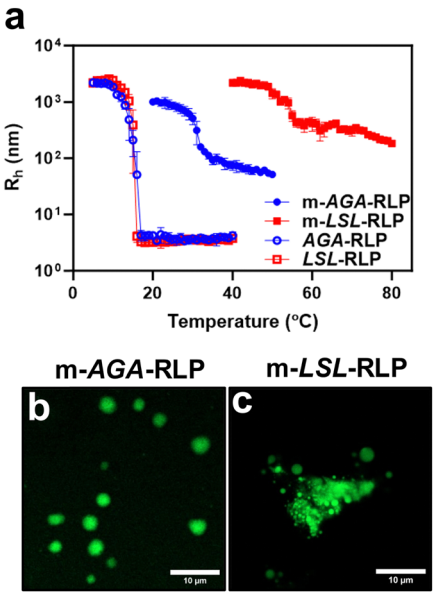

Fig. 3 Characterization of temperature-dependent phase separation and condensate morphology using dynamic light scattering and fluorescent microscopy. (a) Temperature-dependent changes in the hydrodynamic radius of proteins monitored by DLS. Unmodified constructs exhibited sharp aggregation from unimers below their T_c. Lipidated constructs show self-assembly at temperatures higher than T_c, with sizes dependent on the lipidation site sequence. [protein] = 10 μM in PBS, with error bars representing standard deviations from three measurements. (b) and (c) Visualization of the condensates of lipidated constructs using confocal microscopy at 25 °C. [protein] = 100 μM in PBS. See Fig. S10 (ESI†) for non-lipidated samples. m-*AGA*-RLP formed spherical condensates, whereas m-*LSL*-RLP formed clusters of smaller droplets.

lipidated proteins, highlighting the impact of the sequence of the lipidation site upon post-translational modification on the meso-scale architecture and assembly of the condensates. m-*AGA*-RLP formed typical spherical droplets (Fig. 3b), while m-*LSL*-RLP formed a cluster of smaller droplets, suggesting a deviation from standard liquid–liquid phase-separation mechanism (Fig. 3c). The spherical morphology of these structures indicates that they likely originate from LLPS, but they appear to be arrested or hindered in their phase-separation process, possibly due to molecular interactions specific to their lipidation site. This suggests that lipidation, coupled with the specific sequence at the lipidation site, not only promotes LLPS in RLPs but also distinctly influences the morphology and organization of the resultant phase-separated droplets.

Prompted by the appearance of clustered droplets in confocal microscopy, we employed fluorescence recovery after photobleaching (FRAP) to quantitatively assess the fluidity of these droplets. The FRAP results indicated significant variations in fluorescence recovery rates, influenced by both lipidation and the specific lipidation site (Fig. 4), suggesting a direct relationship between the sequence at the lipidation site and the mobility of the condensate structures. For example, the FRAP recovery half-lives for unmodified constructs were consistently short ($\tau_{1/2} = 1.5 \pm 0.2$ seconds) across different lipidation sites. In contrast, lipidated constructs exhibited slower recovery rates,

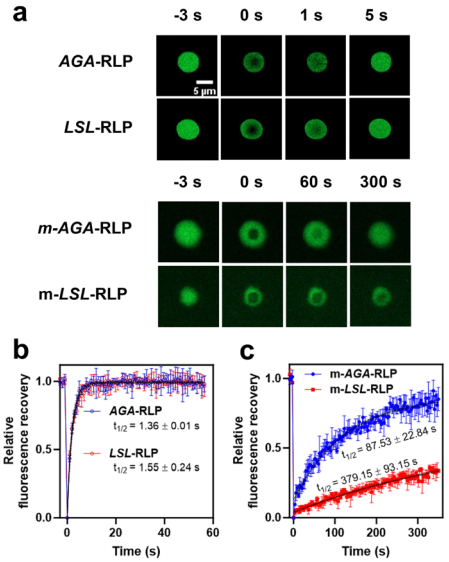

Fig. 4 Characterization of condensate fluidity using fluorescent recovery after photobleaching (FRAP). (a) Output frames from confocal microscopy are presented at various time points: $t = -3$ s before bleaching, immediately after bleaching ($t = 0$ s), and at subsequent intervals post-bleaching to observe recovery. (b) and (c) The FRAP data are normalized and analysed using a single exponential model (see methods for details) to determine the half-life of fluorescence recovery. Two-way ANOVA indicates a statistically significant interaction between the effects of lipidation and lipidation site sequence ($F(1, 8) = 18.47$, $p = 0.0030$). In the absence of lipidation, the recovery is rapid and does not depend on the sequence of the lipidation site (Tukey's HSD, $p > 0.9999$). Lipidation, however, slows the rate of recovery, and the recovery rate of m-*LSL*-RLP is significantly slower than that of m-*AGA*-RLP (Tukey's HSD, $p = 0.0013$).

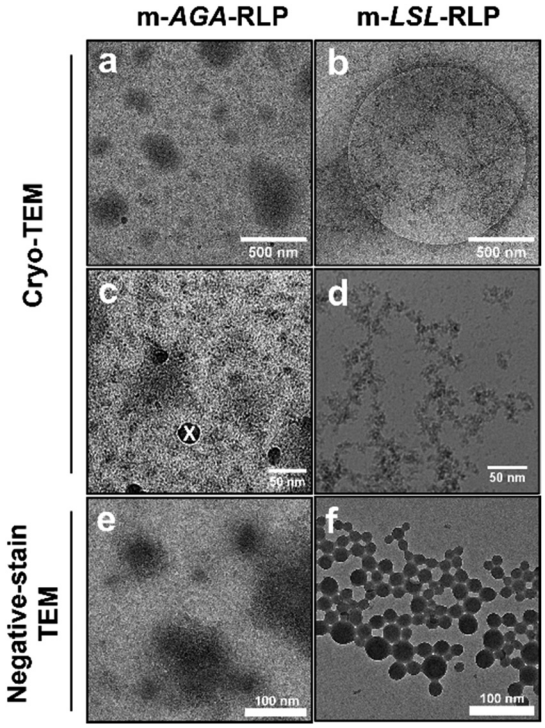

Fig. 5 Nano-scale organization of lipidated RLPs condensates. Cryo-TEM and negative-stain TEM micrographs of m-*AGA*-RLP (a), (c) and (e) and m-*LSL*-RLP (b), (d) and (f) reveal the influence of lipidation sites on the morphology of protein chains within the condensates. m-*AGA*-RLP forms diffuse, shadow-like structures, whereas m-*LSL*-RLP shows clusters of aggregate. An '*x*' marks an ice contamination on the cryo-TEM grid in panel c.

with $\tau_{1/2}$ for m-*AGA*-RLP at 87.5 ± 22.9 seconds and m-*LSL*-RLP displaying much slower rates, with $\tau_{1/2}$ = 379.1 ± 93.2 seconds. This data underscores the complex interplay between the lipid and the sequence of the lipidation site in influencing the material properties of condensates, such as their dynamics and fluidity. Statistical analysis using two-way ANOVA supports this finding ($F(1, 8) = 18.47$, $p = 0.003$). This could be attributed to the formation of structured networks within the condensates. Essentially, if lipidation modifies the assembly of RLPs above the UCST, it could similarly affect the organization of polymer chains within the condensates.

To investigate whether the significantly lower FRAP recovery rates, particularly in m-*LSL*-RLP, indicate network formation within the condensates, we employed transmission electron microscopy (TEM) for detailed nanoscale analysis (Fig. 5). TEM and cryo-TEM imaging revealed distinct properties in m-*LSL*-RLP samples in contrast to other constructs, which exhibited more diffuse, shadow-like appearances on TEM grids. m-*LSL*-RLP uniquely displayed small clusters of spherical aggregates, resembling a 'beads-on-a-string' morphology, indicative of network formation and suggesting a complex, interconnected structure within its condensates. This finding is consistent with the slower FRAP recovery rates for m-*LSL*-RLP, where the network likely restricts molecular mobility, slowing down fluorescence recovery. In m-*AGA*-RLP, while similar distinct structures were not observed, the reduced FRAP recovery rates imply that the lipid motif might still facilitate associative interactions among protein chains in the condensate phase. These interactions, albeit lacking a specific internal arrangement, could limit the dynamics of chain exchange within the condensates.

After showing that the interplay between the lipid and the sequence of the lipidation site alters the phase separation of RLPs, we hypothesized that the molecular mechanisms behind this phenomenon could be due to alterations in the properties of the lipidation site caused by the lipid motifs. These changes might manifest as the formation of structured assemblies (*e.g.*, beta-sheets) or through variations in the hydration levels of residues within the sequence. To delve further into this hypothesis and enhance our understanding of the molecular interactions involved—key to determining the impact of lipidation site sequence on lipidated protein systems—we turned to molecular dynamics (MD) simulations for more comprehensive insights.

To evaluate the interplay between the lipid and the structure of lipidation sites, we analysed the dihedral angles of the peptide backbone for each residue in the lipidation site using Ramachandran plots (Fig. S12, ESI†). This analysis demonstrated that residues at the lipidation sites are scattered across various conformational spaces. This scattering suggests significant conformational flexibility and indicates that lipidation

does not induce rigidity in the peptide structure, irrespective of the sequence of the lipidation site or simulation temperature, consistent with the results of FT-IR spectroscopy (Fig. S13, ESI†).

With structural changes in the lipidation site or RLP domain ruled out as the primary differentiator, we shifted our focus to hydration dynamics. We hypothesized that variations in the lipidation site sequence, in synergy with the attached lipid, can result in altered hydrophobic character extending beyond the lipid itself, leading to different hydration levels within the peptide chain. To explore this hypothesis, we employed a recently developed computational method, protocol for assigning a residue's character on the hydropathy (PARCH) scale.[41] PARCH is a novel computational technique that evaluates protein hydropathy at the residue level by analysing the behaviour of water molecules around a protein's shell at various temperatures. Each residue is assigned a parch value on a 0 to 10 scale, where lower values indicate hydrophobic character. Distinct from traditional hydropathy scales, PARCH allows for nuanced comparisons of hydropathy by accounting for the variable nature of residue hydropathy based on its structural context. Additionally, its computationally efficient methodology proves advantageous for applications in materials design.[30]

The PARCH scale analysis, depicted in Fig. 6 and Fig. S14 (ESI†), highlights hydrophobicity differences at the lipidation sites of m-*AGA*-RLP and m-*LSL*-RLP. Specifically, residues A2-A4 showed lower PARCH values—indicative of higher hydrophobicity—for the LSL sequence. This is in line with the inherently hydrophobic nature of the larger leucine residues. More crucially though, the flanking residues (*e.g.*, G1, S5, and R6) which are identical in both sequences exhibited significant differences in PARCH values. In the case of m-*LSL*-RLP, Gly1 and Ser5 demonstrated markedly increased hydrophobicity, an effect also observed for Arg6 and Gly7. This pattern suggests that the lipidation site's sequence, in conjunction with the lipid, may extend the hydrophobic region, potentially diminishing its water compatibility and thereby enhancing the interactions between lipidated RLPs, either in solution or within the condensate phase.

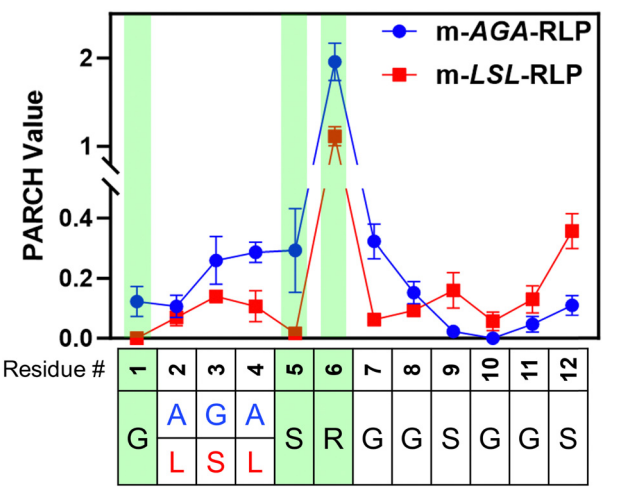

Fig. 6 Computational analysis of lipidation site hydrophobicity using the PARCH scale method. This analysis revealed distinct differences in PARCH values between lipidated RLPs, with m-*LSL*-RLP displaying higher hydrophobicity (denoted by lower PARCH values) compared to m-*AGA*-RLP, even in regions where both constructs share similar amino acid sequences. These findings suggest that the interplay between the lipidation site and lipid may lead to an extended hydrophobic region, likely enhancing the interactions between lipidated RLPs in solution and condensed phases.

Discussion

This study has shown that myristoylation, along with the specific sequences at lipidation sites, markedly influenced the phase separation and material properties of RLPs, a prototypical IDP with UCST-type behaviour. Various experimental techniques have been used to show that lipidation elevated the UCST cloud points and altered the dynamics and fluidity of condensates, with the degree of these effects varying based on the lipidation site sequence. Molecular dynamics simulations indicated that these changes arise not from alterations in peptide rigidity, but likely from the interaction between the lipid and the lipidation site, leading to an expanded hydrophobic region. These findings pave the road for the design of lipidated resilins for biomedical applications such as heat-mediated release of hydrophobic drugs, leveraging their unique amphiphilic and thermo-responsive capabilities.

Our work establishes a crucial framework for understanding the impact of lipidation on the phase separation of proteins exhibiting UCST behaviour. This framework addresses an important gap in the literature because most prior studies on lipidation's effect on protein phase separation have concentrated on lipidated ELPs, which typically exhibit LCST phase behaviour.[30,31] These studies indicate that lipidation lowers the LCST and affects the concentration dependencies of the coexistence curves in the dilute branch of the phase diagram. Our findings contribute to this body of knowledge by demonstrating that lipidation increases the UCST temperature without significantly altering the concentration dependence of the cloud point temperature. This result is significant because LCST-type phase separation is relatively rare in natural systems, with only a few proteins, such as the poly-A binding protein[42] and tau protein,[43] exhibiting this behaviour *in vitro*. While this list is expected to expand, the catalogue of proteins undergoing the UCST-type phase separation is already extensive. We propose that the observed effects of lipidation are likely generalizable to these proteins, including those with complex sequences like FUS, DDX4, and Laf-1. Future research will explore this hypothesis. Additionally, we plan to extend our investigations to examine how lipidation affects the behaviour of systems with dual LCST-UCST properties or reentrant phase transitions.

In this study, we demonstrate that even small alterations to the sequence of the lipidation site—merely three amino acids—result in significant differences in the phase boundaries and material properties of RLP condensates. Importantly, we observe these alterations only after lipidation, indicating that lipidation may enhance secondary interactions at the lipidation sites. Our PARCH analysis suggests that the increased hydrophobicity at the lipidation site might be a critical factor in

enhancing secondary interactions after myristoylation. This observation partially aligns with earlier observations on ELP condensates, where the sequence of the lipidation site did not affect phase boundaries yet altered their morphology and clustering.[44] These findings suggest that the effects of lipidation site sequences on phase behaviour may be more generalizable across proteins exhibiting LCST- or UCST-type phase behaviour.

Importantly, these observations prompt intriguing questions regarding the traditional criteria of classifying PTMs based on the chemical nature of the PTM motif and the modified residue. Our results suggest that this definition may be too narrow, as it overlooks the broader context of surrounding residues. In our study, two lipidated RLPs exhibited distinct properties, even though both were modified with the same group at the same site—highlighting the role of residues in the proximity of the PTM motif. Given that enzymes catalysing PTMs often target proteins with diverse sequences near the PTM sites, it is tempting to consider whether these sequence variations are evolved to prevent cross-reactivity, or they may confer distinct interaction profiles post-modification. Our findings support the potential functional role of these residues to impart unique structural and material characteristics to proteins far beyond their conventional roles as mere enzymatic recognition sites.

Conclusions

Collectively, these findings enhance our understanding of the structural and dynamic intricacies introduced by lipidation, providing insights that could inform future biomaterial design and protein engineering endeavours. We emphasize the need for a more comprehensive examination of the interplay between the lipids and lipidation sites, suggesting the development of libraries with systematic variations in lipidation site sequences. Additionally, extending the use of multi-chain simulations and structural analysis tools such as NMR will be instrumental in elucidating the molecular interactions that define the biophysical properties of lipidated proteins.[45] This integrated approach can elucidate the impacts of this enigmatic class of PTMs, enabling the 'lipo-engineering' of proteins to enhance functional attributes such as allostery and catalysis.

Author contributions

The manuscript was written through the contributions of all authors. All authors have given approval to the final version of the manuscript.

Conflicts of interest

There are no conflicts to declare.

Acknowledgements

DM acknowledges the support of the National Science Foundation CAREER Award (2146168) and the National Institutes of Health (R35GM142899). The computational work was supported by the National Science Foundation (BMAT-2105193, DM and SN) and the National Science Foundation (MCB-2221796, SN). Briah Bailey was supported by the NSF Research Experiences for Undergraduates (REU) program (1950802). The plasmid encoding the gene for RLP was a generous gift from the Chilkoti Lab at Duke University. Confocal microscopy was conducted at the Blatt Bioimaging Center, supported by the NIH (S10 OD026946). Cryo-TEM imaging was performed at the Cornell Center for Materials Research Shared Facilities, funded through the NSF MRSEC program (DMR-1719875). We thank Dr Abrar A. Aljiboury for assistance with confocal microscopy and Dr Mariena S. Ramos for assistance with cryo-TEM imaging.

References

1 C. E. Sing and S. L. Perry, *Soft Matter*, 2020, **16**, 2885–2914.
2 E. Gomes and J. Shorter, *J. Biol. Chem.*, 2019, **294**, 7115–7127.
3 K. O. Margossian, M. U. Brown, T. Emrick and M. Muthukumar, *Nat. Commun.*, 2022, **13**, 2250.
4 E. Ban and A. Kim, *Int. J. Pharm.*, 2022, 122058.
5 L. van Westerveld, J. Es Sayed, M. de Graaf, A. H. Hofman, M. Kamperman and D. Parisi, *Soft Matter*, 2023, **19**, 8832–8848.
6 P. Pullara, I. Alshareedah and P. R. Banerjee, *Soft Matter*, 2022, **18**, 1342–1349.
7 Y. Chao and H. C. Shum, *Chem. Soc. Rev.*, 2020, **49**, 114–142.
8 C. Garcia Garcia and K. L. Kiick, *Acta Biomater.*, 2019, **84**, 34–48.
9 C. E. R. Edwards, K. L. Lakkis, Y. Luo and M. E. Helgeson, *Soft Matter*, 2023, **19**, 8849–8862.
10 J. R. Simon, S. A. Eghtesadi, M. Dzuricky, L. You and A. Chilkoti, *Mol. Cell*, 2019, **75**(66–75), e65.
11 M. Dzuricky, B. A. Rogers, A. Shahid, P. S. Cremer and A. Chilkoti, *Nat. Chem.*, 2020, **12**, 814–825.
12 Z.-G. Qian, S.-C. Huang and X.-X. Xia, *Nat. Chem. Biol.*, 2022, **18**, 1330–1340.
13 E. W. Martin and Tanja Mittag, *Biochemistry*, 2018, **57**, 2478–2487.
14 N. A. Zervoudis and A. C. Obermeyer, *Soft Matter*, 2021, **17**, 6637–6645.
15 B. S. Schuster, G. L. Dignon, W. S. Tang, F. M. Kelley, A. K. Ranganath, C. N. Jahnke, A. G. Simpkins, R. M. Regy, D. A. Hammer, M. C. Good and J. Mittal, *Proc. Natl. Acad. Sci. U. S. A.*, 2020, **117**, 11421–11431.
16 J. R. Simon, N. J. Carroll, M. Rubinstein, A. Chilkoti and G. P. Lopez, *Nat. Chem.*, 2017, **9**, 509–515.
17 B. S. Schuster, E. H. Reed, R. Parthasarathy, C. N. Jahnke, R. M. Caldwell, J. G. Bermudez, H. Ramage, M. C. Good and D. A. Hammer, *Nat. Commun.*, 2018, **9**, 2985.
18 J. Dhandhukia, I. Weitzhandler, W. Wang and J. A. MacKay, *Biomacromolecules*, 2013, **14**, 976–985.
19 Y. Shin, J. Berry, N. Pannucci, M. P. Haataja, J. E. Toettcher and C. P. Brangwynne, *Cell*, 2017, **168**(159–171), e114.
20 K. W. Barber and J. Rinehart, *Nat. Chem. Biol.*, 2018, **14**, 188–192.

21 W. T. Snead and A. S. Gladfelter, *Mol. Cell*, 2019, **76**, 295–305.
22 M. Hofweber and D. Dormann, *J. Biol. Chem.*, 2019, **294**, 7137–7150.
23 B. Tsang, J. Arsenault, R. M. Vernon, H. Lin, N. Sonenberg, L.-Y. Wang, A. Bah and J. D. Forman-Kay, *Proc. Natl. Acad. Sci. U. S. A.*, 2019, **116**, 4218–4227.
24 T. H. Kim, B. Tsang, R. M. Vernon, N. Sonenberg, L. E. Kay and J. D. Forman-Kay, *Science*, 2019, **365**, 825–829.
25 Q. Wang, Z. Li, S. Zhang, Y. Li, Y. Wang, Z. Fang, Y. Ma, Z. Liu, W. Zhang and D. Li, *Proc. Natl. Acad. Sci. U. S. A.*, 2022, **119**, e2205255119.
26 M. Saito, D. Hess, J. Eglinger, A. W. Fritsch, M. Kreysing, B. T. Weinert, C. Choudhary and P. Matthias, *Nat. Chem. Biol.*, 2019, **15**, 51–61.
27 H. Jiang, X. Zhang, X. Chen, P. Aramsangtienchai, Z. Tong and H. Lin, *Chem. Rev.*, 2018, **118**, 919–988.
28 R. A. Kapelner, V. Yeong and A. C. Obermeyer, *Curr. Opin. Colloid Interface Sci.*, 2021, **52**, 101407.
29 M. S. Hossain, Z. Zhang, S. Ashok, A. R. Jenks, C. J. Lynch, J. L. Hougland and D. Mozhdehi, *ACS Appl. Bio Mater.*, 2022, **5**, 1846–1856.
30 J. Ji, M. S. Hossain, E. N. Krueger, Z. Zhang, S. Nangia, B. Carpentier, M. Martel, S. Nangia and D. Mozhdehi, *Biomacromolecules*, 2023, **24**, 1244–1257.
31 T. Zhang, F. Peruch, A. Weber, K. Bathany, M. Fauquignon, A. Mutschler, C. Schatz and B. Garbay, *RSC Adv.*, 2023, **13**, 2190–2201.
32 S. Saha, S. Banskota, S. Roberts, N. Kirmani and A. Chilkoti, *Adv. Ther.*, 2020, **3**, 1900164.
33 F. G. Quiroz and A. Chilkoti, *Nat. Mater.*, 2015, **14**, 1164–1171.
34 R. Balu, N. K. Dutta, A. K. Dutta and N. R. Choudhury, *Nat. Commun.*, 2021, **12**, 149.
35 S. Patkar, N. Jovic, J. Mittal and K. Kiick, *ACS Biomater. Sci. Eng.*, 2021, **7**, 4244–4257.
36 S. Maurer-Stroh, B. Eisenhaber and F. Eisenhaber, *J. Mol. Biol.*, 2002, **317**, 523–540.
37 D. E. Meyer and A. Chilkoti, *Biomacromolecules*, 2004, **5**, 846–851.
38 Z. Zhang, C. J. Lynch, Y. Huo, S. Chakraborty, P. S. Cremer and D. Mozhdehi, *J. Am. Chem. Soc.*, 2024, **146**(8), 5383–5392.
39 K. M. Luginbuhl, D. Mozhdehi, M. Dzuricky, P. Yousefpour, F. C. Huang, N. R. Mayne, K. L. Buehne and A. Chilkoti, *Angew. Chem., Int. Ed.*, 2017, **56**, 13979–13984.
40 V. Zai-Rose, S. J. West, W. H. Kramer, G. R. Bishop, E. A. Lewis and J. J. Correia, *Biophys. J.*, 2018, **115**, 1431–1444.
41 J. Ji, B. Carpentier, A. Chakraborty and S. Nangia, *J. Chem. Theory Comput.*, 2024, **20**(4), 1656–1672.
42 J. A. Riback, C. D. Katanski, J. L. Kear-Scott, E. V. Pilipenko, A. E. Rojek, T. R. Sosnick and D. A. Drummond, *Cell*, 2017, **168**(1028–1040), e1019.
43 S. K. Rai, A. Savastano, P. Singh, S. Mukhopadhyay and M. Zweckstetter, *Protein Sci.*, 2021, **30**, 1294–1314.
44 D. Mozhdehi, K. M. Luginbuhl, J. R. Simon, M. Dzuricky, R. Berger, H. S. Varol, F. C. Huang, K. L. Buehne, N. R. Mayne, I. Weitzhandler, M. Bonn, S. H. Parekh and A. Chilkoti, *Nat. Chem.*, 2018, **10**, 496–505.
45 N. L. Fawzi, S. H. Parekh and J. Mittal, *Curr. Opin. Struct. Biol.*, 2021, **70**, 78–86.